Title

Rapidly polymerizing injectable click hydrogel therapy to delay bone growth in a murine re-synostosis model

Journal

Biomaterials, 35(36)

ISSN

0267-6605

Authors

Hermann, Christopher D
Wilson, David S
Lawrence, Kelsey A
et al.

Publication Date

2014-12-01

DOI

10.1016/j.biomaterials.2014.07.065

Peer reviewed

Published in final edited form as:
Biomaterials. 2014 December ; 35(36): 9698–9708. doi:10.1016/j.biomaterials.2014.07.065.

Rapidly Polymerizing Injectable Click Hydrogel Therapy to Delay Bone Growth in a Murine Re-synostosis Model

Christopher D. Hermann[1,2,†], **David S. Wilson**[1,†], **Kelsey A. Lawrence**[1], **Xinghai Ning**[1], **Rene Olivares-Navarrete**[3], **Joseph K. Williams**[4], **Robert E. Guldberg**[5], **Niren Murthy**[*,6], **Zvi Schwartz**[6], and **Barbara D. Boyan**[*,1,3]

[1]Wallace H. Coulter Department of Biomedical Engineering, Georgia Institute of Technology Atlanta, GA

[2]Emory University School of Medicine, Atlanta, GA

[3]Department of Biomedical Engineering, School of Engineering, Virginia Commonwealth University, Richmond, VA

[4]Children's Healthcare of Atlanta, Atlanta, GA

[5]Woodruff School of Mechanical Engineering, Georgia Institute of Technology Atlanta, GA

[6]Department of Bioengineering, University of California at Berkeley, Berkeley, CA

Abstract

Craniosynostosis is the premature fusion of cranial sutures, which can result in progressive cranial deformations, increased intracranial pressure, and restricted brain growth. Most cases of craniosynostosis require surgical reconstruction of the cranial vault with the goal of increasing the intracranial volume and correcting the craniofacial deformities. However, patients often experience rapid post-operative bone re-growth, known as re-synostosis, which necessitates additional surgical intervention. Bone morphogenic protein (BMP) inhibitors have tremendous potential to treat re-synostosis, but the realization of a clinically viable inhibitor-based therapeutic requires the development of a delivery vehicle that can localize the release to the site of administration. Here, we present an in situ rapidly crosslinking injectable hydrogel that has the properties necessary to encapsulate co-administered proteins and demonstrate that the delivery of rmGremlin1 via our hydrogel system delays bone re-growth in a weanling mouse model of re-synostosis. Our hydrogel is composed of two mutually reactive poly(ethylene glycol) macromolecules, which when mixed crosslink via a bio-orthogonal Cu free click reaction. Hydrogels containing Gremlin caused a dose-dependent inhibition of bone regrowth. In addition to

[*]To whom correspondence should be addressed: Barbara D. Boyan, Ph.D., Dean, School of Engineering, Virginia Commonwealth University, 601 West Main Street, Suite 331, Richmond, Virginia 23284-3068, Phone: 804-828-0190, bboyan@vcu.edu. Niren Murthy, Ph.D., Department of Bioengineering, University of California at Berkeley, Hearst Memorial Mining Building, Berkeley CA, 94720, nmurthy@berkeley.edu.
[†]Contributed equally to the publication

craniofacial applications, our injectable click hydrogel has the potential to provide customizable protein, small molecule, and cell delivery to any site accessible via needle or catheter.

Keywords

Bone ingrowth; Hydrogel; BMP (bone morphogenetic protein); Craniosynostosis; Re-synostosis

1. Introduction

Craniosynostosis is the pathologic premature fusion of the cranial sutures early in development, affecting nearly 1 in 2000 children [1–4]. If left untreated, craniosynostosis can result in progressive craniofacial deformities, restricted brain growth, and an increase in intracranial pressure (ICP), which may cause central nervous system complications such as blindness, deafness, seizures, and in extreme cases death [5–9]. The standard treatment for most cases of craniosynostosis is complex cranial vault reconstruction, wherein surgeons remove the majority of the calvaria and reshape the bones to increase the intracranial volume and correct the craniofacial deformities. In up to 10–40% of children, bone rapidly re-grows following surgery, resulting in a condition called re-synostosis [10,11]. This re-synostosis can result in a subsequent increase in intracranial pressure and other nervous system complications. These patients frequently undergo subsequent cranial vault reconstructions, which are associated with a high incidence of life threatening complications including meningitis, encephalitis, and intracranial hemorrhage [12,13]. Despite the frequency and severity associated with the treatment of re-synostosis, there are no clinically viable therapies to control or prevent rapid post-operative cranial fusion.

The earliest treatment for re-synostosis involved placing a variety of physical barriers in the spaces created during surgery. These procedures were abandoned because these materials resulted in an increase in infections with no substantial delay in bone growth [14]. As a result, any therapy designed to delay re-synostosis must target the biological processes that are responsible for rapid bone formation. Prior work with both rabbit and adult murine models has attempted to prevent post-operative bone growth [15–18]. These methods have primarily used collagen-based vehicles or ex-vivo based therapies to control the post-operative bone growth.

One of the major challenges when delivering any biologically active molecule is rapid diffusion away from the sight of administration. This makes it impossible to sustain therapeutic concentrations of the active molecules via bolus injection within the defects created during cranial vault surgery. Given their ability to conform to the shape of tissue defects and localize the continuous release of proteins to the site of administration, injectable in situ crosslinking hydrogels are ideal platforms for the sustained delivery of biologically active molecules. Injectable hydrogels are composed of mutually reactive soluble precursors that react in situ to form insoluble networks. In addition, due to their high water content, hydrogels are well suited for the delivery of proteins and other biomolecules that can be denatured upon contact with hydrophobic surfaces [19].

Traditional gelation chemistries that are based on free radical polymerization, Michael addition, or amide bond formation, are either too slow to encapsulate co-delivered proteins before they diffuse away from the site of administration, or use initiators and precursors that react with cellular components and can be toxic to neuronal and skeletal tissues [20–26]. “Click chemistry” and other bio-orthogonal gelation mechanisms have great promise for in situ hydrogel formation, due to their rapid polymerization kinetics and low reactivity with cellular components. However, the development of catalyst-free click chemistry-based gelation mechanisms for protein release in vivo remains a major challenge. Thus, there is great interest in developing new injectable hydrogels based on click chemistry that can deliver proteins in vivo [27,28].

Bone morphogenetic protein (BMP) antagonists are attractive therapeutic proteins for controlling the rate of bone growth as they are normally secreted extracellularly to control the activity of BMP [29,30]. BMP is produced by osteoblast-lineage cells and acts in an autocrine/paracrine manner to stimulate bone formation. Activity of BMP is tightly controlled in vivo via a complex set of regulatory strategies involving availability of inhibitors, receptor subunits, and intracellular signaling mediators. Endogenous BMP inhibitors are secreted extracellularly and function by binding to the target BMP molecule and in turn preventing BMP receptor activation. BMP-inhibitors are differentially expressed during the rapid bone growth that occurs following the surgical removal of the posterior frontal suture in weanling mice [31]. One of these inhibitors, Gremlin is an attractive BMP inhibitor for use in delaying re-synostosis as it is up regulated prior to the BMP2 and BMP4 mediated mineralization seen in a weanling murine model of re-synostosis [31]. In contrast, the widely studied antagonist Noggin was upregulated following the completion of mineralization of the cranial defect [15,16,31,32]. As a result, we hypothesized that Gremlin would be a more effective inhibitor as it was involved in the cartilage to mineralized tissue transition early in defect healing.

Here, we present a bio-orthogonal injectable hydrogel that is designed to crosslink to completion in less than two minutes and should thus have the gelation kinetics needed for in situ encapsulation and subsequent delivery of the BMP inhibitor rmGremlin1. In order to achieve such rapid network formation, we synthesized multivalent poly(ethylene glycol) precursors (Figure 1A, 1 & 2) that form an insoluble network upon mixing (Figure 1A, 3) via the ring-strain promoted Cu-free click reaction between dibenzylcyclooctynes (DBCO) and azides. Our hydrogel system also contains ester linkages to ensure that the system is ultimately degraded and excreted, which we anticipate will happen on the timescale of weeks. We selected the DBCO-azide reaction for in situ gelation because it is two orders of magnitude faster than previously reported click-based gelation mechanisms, proceeds under physiological conditions, and is non-toxic to cells [33]. Using a cranial defect over the posterior frontal suture of weanling mice, we investigated the ability of our hydrogel system to release therapeutic concentrations of active Gremlin1 by examining the effects of sustained release of the protein over 14 days on inhibition of the rapid post-operative bone growth that occurs with this model.

2. Materials and Methods

2.1 Synthesis of tetraethylene glycol methacrylate (TEGMA)

Tetraethylene glycol (5.0g, 25.7 mmol), and pyridine (2.0 g, 25.3 mmol) were added to anhydrous dichloromethane (DCM) (100 ml) in a 250 ml flask and stirred for 30 min at 0°C. Methacryloyl chloride (2.6 g, 25 mmol) was added drop-wise to the stirred solution. The reaction was allowed to stir at 0°C for 2 h, and then at room temperature (rt) for an additional 2 h. The reaction was then concentrated via rotary evaporation, re-suspended in ethyl acetate, and finally evaporated onto silica gel. The mono methacrylate product was separated from the di-methacrylate byproduct and starting material via flash silica gel chromatography on silica gel using a mixture of ethyl acetate and hexanes (7:3). 1H NMR (300 MHz, CDCl3) δ 2.01 (t, *J* = 6.0 Hz, 3H, CH3), 2.82(t, *J* = 6.0 Hz, 1H, OH), 3.49–3.65 (m, 16H, 8 × CH2), 6.48 (m, 2H, CH2=C); 13C NMR (75.5 MHz, CDCl3) δ 167.32 (C=O), δ 136.0 (C=CH2), 125.87 (CH2=C), 61.51 (*C*H2OH), 69.91 (CH2), 70.21 (CH2), 70.46 (CH2), 70.52 (CH2), 70.56 (CH2), 72.43 (CH2), 39.23 (C), 17.83 (CH3).

2.2 Synthesis of tetraethylene glycol mono 4-methylbenzenesulfonate

Tetraethylene glycol (5.0g, 25.7 mmol) and pyridine (2.0 g, 25.3 mmol) were added to anhydrous dichloromethane (100 ml) in a 250 ml flask and stirred for 30 min at 0°C. A solution of 4-toluenesulfonylchloride (4.75, 20 mmol) in 30 ml DCM was added drop-wise via syringe pump to the flask. The reaction mixture was then stirred for 2 h at 0°C, then another 4 hours at rt. The reaction mixture was then poured into ice water and the organic layer was separated then washed 2X with brine and dried over $MgSO_4$ before being concentrated via rotary evaporation. The crude product was then re-suspended in ethyl acetate and evaporated onto silica gel. The mono tosylated product was separated from the di-tosylated byproduct and starting material via flash silica gel chromatography using a mixture of ethyl acetate and hexanes (6:4). 1H NMR (300 MHz, CDCl3) δ 2.33 (s, 3H, CH3), 2.89 (t, *J* = 6.0 Hz, 1H, OH), 3.42–3.70 (m, 14H, 7×CH2), 4.00–4.12 (m, 2H, C*H*2OTs), 7.24 (d, *J* = 8.0 Hz,2H, 2×Hm), 7.68 (d, *J* = 8.0 Hz, 2H, 2×Ho); 13C NMR (75.5 MHz, CDCl3) δ 21.41 (CH3), 61.40 (*C*H2OH), 68.44 (*C*H2OTs), 69.17 (CH2), 70.10 (CH2), 70.22 (CH2), 70.41 (CH2), 70.46 (CH2),72.34 (CH2), 127.73 (2×CHo), 129.68 (2×CHm), 132.76 (C), 144.68 (C).

2.3 Synthesis of tetraethylene glycol mono azide

Sodium azide (2.0 g, 30.76 mmol) was added to a solution of tetraethylene glycol mono 4-methylbenzenesulfonate (2.0 g, 5.74 mmol) in dimethylformamide (100 mL) at room temperature. The reaction mixture was stirred overnight at 90 °C. The reaction was then filtered and concentrated via rotary evaporation. The crude product was added to cold water and extracted with ethyl acetate (4×100 mL). The combined organic layers were then dried over $MgSO_4$ and concentrated under vacuum. The viscous liquid was then purified by flash column chromatography on silica gel using a mixture of ethyl acetate and hexanes (6:4) to yield the desired product as a colorless oil (1.63 g, 81%): 1H NMR (300 MHz, CDCl3) δ 2.91 (t, *J* = 6.0 Hz, 1H, OH), 3.30 (t, *J* = 5.0 Hz, 2H, C*H*2N3), 3.49–3.65 (m, 14H, 7×CH2); 13C NMR (75.5 MHz, CDCl3) δ 50.54 (*C*H2N3), 61.51 (*C*H2OH), 69.91 (CH2), 70.21 (CH2), 70.46 (CH2), 70.52 (CH2), 70.56 (CH2), 72.43 (CH2).

2.4 Synthesis of azido tetraethylene glycol methacrylate (ATEGMA)

Tetraethylene glycol mono azide (2.0g, 9.13 mmol) and pyridine (2.0 g, 25.3 mmol) were added to anhydrous dichloromethane (DCM) (100 ml) in a 250 ml flask and stirred for 30 min at 0°C. Methacryloyl chloride (2.6 g, 25 mmol) was added drop-wise to the stirred solution. The reaction was allowed to stir at 0°C for 2 h, and then at room temperature for an additional 2 h. The reaction was then concentrated via rotary evaporation, re-suspended in ethyl acetate, and finally evaporated onto silica gel. The mono methacrylate product was separated from the starting material via flash silica gel chromatography on silica gel using a mixture of ethyl acetate and hexanes (4:6 v/v). 1H NMR (300 MHz, CDCl3) δ 2.01 (t, *J* = 6.0 Hz, 3H, CH3), 2.91 (t, *J* = 6.0 Hz, 1H, OH), 3.30 (t, *J* = 5.0 Hz, 2H, C*H*2N3), 3.49–3.65 (m, 14H, 7 × CH2), 6.48 (m, 2H, CH2=C); 13C NMR (75.5 MHz, CDCl3) δ 167.32 (C=O), 136.0 (C=CH2), 125.87 (CH2=C), 50.54 (*C*H2N3), 61.51 (*C*H2OH), 69.91 (CH2), 70.21 (CH2), 70.46 (CH2), 70.52 (CH2), 70.56 (CH2), 72.43 (CH2), 39.23 (C), 17.83 (CH3).

2.4 Synthesis of poly [tetraethylene glycol methacrylate)-co-(azidotetraethylene glycol methacrylate)] (PEG-N3) (1)

Tetraethylene glycol methacrylate (0.9 g, 3.43 mmol) and azido tetraethylene glycol methacrylate (0.28g, 1.0 mmol), benzothioylsulfanyl acetic acid (6.27 mg, 0.03 mmol), and azobisisobutyronitrile (AIBN, 0.5 mg, 0.003 mmol) were combined in dimethylformamide (1.5 ml). The reaction flask was degassed via four freeze-pump-thaw cycles, and then immersed in an oil bath and stirred at 70°C. After 20 h, the reaction was terminated by flash freezing in liquid nitrogen. The reaction product was added to dichloromethane (DCM) (5 ml) and then precipitated via the addition of methanol (25ml). The supernatant was decanted and the precipitated polymer was subjected to three more rounds of resuspension and precipitation before being concentrated under reduced pressure. The purified polymer was analyzed for weight by gel permutation chromatography (tetrahydrofuran) and the structure and purity were verified by ^{1}H NMR (deuterated chloroform) to have a molecular weight of Mw ~ 24 kDa, Mn ~ 18 kDa (Supplementary Figure 1).

2.5 Synthesis of 4-dibenzocyclooctynol PEG conjugate (PEG-DBCO) (2)

To a stirred solution of poly(ethylene glycol) bis(amine)$_{3400}$ (340 mg, 0.1 mmol) and NEt_3 (40 mg, 0.4 mmol) in DCM (15 mL) was added benzyl-2-nitro-carbonate functionalized DBCO (90 mg, 0.23 mmol) under an atmosphere of argon. The reaction mixture was kept stirring overnight at ambient temperature, and the solvent was removed under reduced pressure. The residue was dissolved in DCM (30 mL), and washed with water (5 mL) and brine (5 mL). The organic phase was dried over Na_2SO_4, filtered, and evaporated to dryness under reduced pressure. The residue was purified by flash column chromatography on silica gel (DCM/CH_3OH, 15/1) to afford (2) (0.31g, 81.3%) and analyzed by H-NMR. 1H NMR (400 MHz, $CDCl_3$) *δ (ppm)* 3.13-3.03 (m, 4H, CH_2CHO), 3.50–3.75 (m, 300H, 150 PEG CH_2), 5.42–5.61 (m, 2H, OC*H*CH_2), 7.21–7.46 (m, 16H, aromatic); and 13C NMR (100 MHz, $CDCl_3$) *δ (ppm)* 40.83(*C*H_2CH), 46.08 (*C*H-O), 69.88 (*C*H_2), 70.19 (*C*H_2), 70.46 (*C*H_2), 76.58 (*C*H_2), 77.50 (*C*H_2), 109.91 (alkyne), 112.78 (alkyne), 121.12 (aromatic), 123.68 (aromatic), 123.73 (aromatic), 125.78 (aromatic), 126.07 (aromatic), 126.94

(aromatic), 127.85 (aromatic), 127.96 (aromatic), 129.85 (aromatic), 150.92 (aromatic), 152.12 (C=O), 155.41(C=O).

2.6 In vitro hydrogel testing

All in vitro experiments were performed under aseptic conditions. Aqueous stock solutions of PEG-DBCO (12.5%, 6.25%, 4.85%, 3.13%, 1.56%; w:v) and PEG-N3 (50%; w:v) were prepared by sonicating the polymers in PBS at room temperature. Two parts PEG-DBCO and 1 part PEG-N3 were incubated on ice until mixing by pipetting and injected in to a modified syringe mold. The gels were then incubated at 37 °C in 1 mL of PBS with 10% FBS until testing. Unconstrained compression testing was performed with the samples immersed in PBS, a 0.1 ± 0.01 N preload, a displacement of 3 mm, and a 2 mm/s compression velocity (Bose EnduraTEC 3100, Bose Corporation, Eden Prairie, Minnesota). GST was fluorescently labeled with Alexa Fluor 647 carboxylic acid, succinimidyl ester using the manufactures protocol, purified with a PD 10 column, lyophilized overnight, and re-suspended in sterile PBS. Aliquots were diluted 1:5 v/v in sterile PBS and quantified by fluorometry. The biological activity of rmGremlin1 delivered from the 12.5% w:v hydrogel was performed by incubating gels containing 100 ng rmGremlin1 or 4 nM HCl vehicle were incubated at 37 °C for 7 days in DMEM. Serum and 100 ng/mL rhBMP2 or vehicle were added to incubated medium and added to MG63 cells at 80% confluence. After 24 hours, cells were harvested and alkaline phosphatase activity was measured in cell layer lysates as previously described [34].

2.7 In vivo testing

All calvarial defects were created in post-natal day 21 male C57Bl/6J mice. Under 28X magnification a 1.5 mm by 2.5 mm defect was made by removing the posterior frontal suture using a piezoelectric instrument under constant irrigation with sterile PBS as previously described [31]. The defects were left empty or injected with 2 μL of the 12.5% hydrogel with the appropriate concentration of rmGremlin1 or GST-647. The ratios and mixing were performed as described above and the polymerization was verified after 20 seconds with a blunt 25G needle. All mice were randomized to both treatment group and post-operative time point with all analysis conducted by a blinded reviewer. Fluorescence release from mice containing hydrogel + GST-647 or PEG-N3 + GST-647 was assessed in anesthetized animals on post-operative days 0, 2, 5, and 14 (IVIS Lumina II) (2 groups, n=5). Total fluorescent counts over the entire head and in a 1.5 mm by 2.5 mm area were determined using the same display scales.

The effect of rmGremlin1 delivered from the hydrogel was assessed by creating the cranial defects described above. Defects were randomized to contain 2 μL of: empty defect, hydrogel only, hydrogel + 300 ng rmGremlin1, hydrogel + 500 ng rmGremlin1, and the unpolymerized PEG-N3 + 500 ng rmGremlin1 (5 groups, n=10). On post-op days 5 and 14, mice were euthanized and imaged with μCT with a voxel size of 31 μm (VivaCT 40, Scanco Medical, Basel, Switzerland). The extent of bone regeneration in the defect was assessed using our advanced segmentation algorithm described and validated previously [31,35]. Histological assessment was performed by hematoxylin and eosin (H&E) staining of decalcified 7 μm axial sections in the middle of the defect and analyzed by light microscopy.

2.8 Histomorphometric analysis

After imaging with μCT the samples were thawed and the brain was removed taking care not to damage the defect. The samples were fixed in 10% neutral buffered formalin, changing the solution after 24 hours. The skulls were decalcified using 10% EDTA changing the solution every 48–72 hours for a period of approximately 3 weeks. Complete de-calcification was verified on a plain x-ray. Under 4x magnification the center of the defect was visualized and a coronal cut was made through the center of the defect. The samples were dehydrated with ethanol and embedded in paraffin. Sections 7 μm in thickness were made and stained with H&E using standard protocols. The samples were imaged at 10x magnification and the bone was manually segmented by a blinded reviewer. The average defect width and average thickness of the bones were calculated (Matlab).

2.8 Statistical analysis

All data are represented as the mean ± standard error of the mean. The sample size for all in vivo and in vitro experiments was determined by a prospective power analysis based on previously reported data. All cell culture experiments were performed with six independent cultures (n=6) and repeated two times. All in vivo experiments were performed in 5 mice per group per time point (n=5). The normality of the data was verified by the D'Agistino-Pearson omnibus normality test. For all in vitro experiments, a one way ANOVA was performed and where appropriate significance among groups was determined by a multiple comparison test with Bonferroni adjustments. For all in vivo experiments a two way ANOVA was performed and as expected there a significant ($P<0.001$) effect of treatment group, time, and interaction for all analysis. Since interactions were found significant, main effect significance was tested by either a conditional one way ANOVA with Bonferroni multiple comparison post-test or an un-paired two-sided t-test not assuming equal variance. Statistical significance for all experiments was declared when the p-value was less than 0.05.

All procedures were approved by the Georgia Tech Institutional Animal Care and Use Committee in accordance with the guide for the Care and Use of Laboratory Animals.

3. Results

3.1 Hydrogel polymerization kinetics and mechanical testing

To generate a water-soluble non-fouling multivalent azide functionalized polymer, we synthesized PEG-N_3 (Figure 1A, 1) from azide functionalized and non-functionalized PEG methacrylate monomers via reversible addition-fragmentation chain transfer (RAFT) polymerization, which affords tight control of azide functionality. The synthetic strategy presented here generates polymers with molecular weights (M_N) of approximately 25,000 Da and average azide functionality per polymer of 13 (Supplemental Figure S1). The difunctionalized PEG-DBCO crosslinker (Figure 1A, 2) was synthesized by reacting bis-amino-PEG with excess benzyl-2-nitro-carbonate functionalized DBCO. Dynamic time sweep rheological experiments were conducted on gels formed in the presence of serum to monitor network formation kinetics. Upon mixing, hydrogels containing 12.5% PEG-N3 and 4% PEG-DBCO underwent gelation in less than 30 seconds (i.e. $G' = G''$) and were completely crosslinked in under 90 seconds (Figure 1B). This rapid polymerization permits

rapid encapsulation and sequestration of co-delivered proteins before they can diffuse away from the site of administration.

One of the advantages of synthetic hydrogels is that the mechanical properties can be tailored to match different tissue types, allowing for better incorporation of the material. Varying the relative concentration of PEG-DBCO prior to polymerization enabled the formation of gels with highly customizable mechanical properties. To generate gels for in vitro evaluation, PBS solutions containing either PEG-DBCO (50%; w:v) or PEG-N_3 (12.5%, 6.25%, 4.85%, 3.13%, 1.56%; w:v) were mixed via pipette in a cylindrical form. As with most hydrogels, our gel displayed a highly non-linear behavior in response to compression [36]. A neo-Hookean hyperelastic model assuming incompressibility and isotropy was used to fit the non-linear stress-strain response of our gels (Supplemental Figure S2). The neo-Hookean coefficient (C_1) was calculated in terms of the stretch ratio (λ)and the engineering stress in the axial direction (σ_{11}^{eng}):$\sigma_{11}^{eng}=2C_1(\lambda-\frac{1}{\lambda^2})$. Unconstrained compression testing showed that increasing the concentration of PEG-DBCO resulted in an increase in the mechanical properties of the hydrogel (Figure 2A). At the lowest concentration, the neo-Hookean coefficient was less than 0.3. It increased to approximately 2 for the mid concentrations, and then finally peaked at over 5 for the 12.5% PEG-DBCO. For 12.5% gels, this corresponded to a Young's modulus of approximately 32 kPA. Hydrogels with concentrations less than 1.5% or greater than 12.5% did not polymerize (data not shown).

3.2 In vitro release kinetics from hydrogel

One of the most important aspects of delivery matrices is the ability to tailor the release kinetics of therapeutic factors based on the intended application. Varying the PEG-DBCO concentration from 3.13–12.5% in the gel enables substantial variation in protein release rate. To assess protein release kinetics, Alexa Fluor tagged glutathione s-transferase (GST-647) was added to the PEG-DBCO solution prior to polymerization. This protein has a molecular weight similar to the Gremlin1 dimer. To mimic the conditions at the treatment site, in vitro release kinetics were assessed by incubating hydrogels containing GST-647 for up to two weeks in sterile PBS containing 10% FBS at 37°C. Our results demonstrated that the GST-647 release rate from the hydrogel was inversely proportional to the crosslink density of the gel (Figure 2B). For example, hydrogels formulated with less crosslinker had a more rapid and non-linear release of incorporated proteins with the 3.1% gel releasing nearly 75% of the protein after only 1 day. In contrast, gels composed of 12.5% crosslinker had a nearly linear release profile out to 14 days. The compressive moduli of the hydrogels were retained for 3 days of incubation, before gradually decreasing for the remaining time points (Figure 2C).

3.3 Biological activity of co-administered proteins released from hydrogel

Gremlin1 mRNA is upregulated during cranial defect healing coincident with increased expression of Bmp2 and Bmp4, suggesting it plays a specific role in regulating bone formation at this time [31]. Gremlin1 is an extracellular BMP inhibitor that has a high affinity for BMP2 and BMP4 and blocks their action by preventing these proteins from binding their receptors, thereby inhibiting their differentiation into osteoblasts [37]. For this

reason, we hypothesized that the controlled release of Gremlin1 following suturectomy would delay post-operative re-synostosis. To verify that Gremlin1 retains its biological activity following in situ polymerization and subsequent release, we assessed the ability of rmGremlin1 released from the hydrogel to block the action of rhBMP2 in vitro. Delivery of rmGremlin1 in the hydrogel blocked the stimulatory effects of rhBMP2 on osteoblastic differentiation of pre-osteoblast MG63 cells, using alkaline phosphatase specific activity of the cultures as an outcome measure [38,39]. The use of rhBMP2 and MG63 cells was based on the manufacturer's assay to verify the activity of rmGremlin1. Preliminary dose response experiments showed that 100 ng/mL rmGremlin1 was able to block the stimulatory effect of a 24h treatment with 100 ng/mL rhBMP2 on alkaline phosphatase activity (Supplemental Figure S3). Moreover, rmGremlin1 retained biological activity over time when delivered via the hydrogels. Hydrogels containing 100 ng/mL rmGremlin1 or the rmGremlin1 carrier (i.e. 4mM HCl) were incubated in medium for 7 days to achieve release of incorporated proteins. MG63 cells treated with rhBMP2 alone or with rhBMP2 plus the hydrogel with carrier caused the expected increase in alkaline phosphatase compared to control cultures and cultures grown with the hydrogel alone. Addition of rmGremlin1 directly to the rhBMP-2 treated cultures or delivered in the polymerized hydrogel blocked the stimulatory effect of rhBMP2 (Figure 2D). These results demonstrate that co-administered biologically active proteins can be delivered with the hydrogel and retain their biological activity when polymerized in the hydrogel.

3.4 In vivo release kinetics and performance of hydrogel

Given the ability of our hydrogel to encapsulate and release biologically active proteins, we assessed its ability to localize the continuous release of proteins within the weanling murine cranial defect following in situ polymerization. The cranial defect model involves removing the posterior frontal suture in a 21-day-old C57Bl/6 mouse [31]. Following creation of the defect, mice were randomized into two treatment groups. Mice received either an injection of a solution containing PEG-N3, GST-647, and PEG-DBCO (i.e. polymerized gel) or a solution containing PEG-N3 and GST-647 (i.e. unpolymerized gel). The gels have a low viscosity prior to polymerization and visual inspection revealed that the solution was able to fill the entire defect before crosslinking into a stable gel. Our results demonstrate that the crosslinked hydrogel was able to retain the fluorescent signal in the defect site and provide controlled release for up to 14 days (Figs. 3A–D). In contrast, the fluorescent signal in animals containing the un-polymerized PEG-N3 showed that the protein diffused out of the defect as early as 2 days post-op and there was essentially no signal seen on days 5 and 14 post-op (Figs. 3E–H). Quantification of the total fluorescent signal over the head of the animals showed no differences at 0 and 2 days, but there was less total fluorescent signal in the PEG-N3 mice for the later time points on post-op days 5 and 14, indicating that the hydrogel provided a more controlled release of the incorporated protein (Figure 3I). Additionally, the ratio between the signal contained within the defect to the total signal detected at each time point was approximately 1 for the mice treated with the hydrogel, indicating that essentially all of the fluorescent protein was localized to the defects containing the hydrogel (Figure 3J). Defects containing just the un-polymerized PEG-N3 started out having a ratio of approximately 1, but this more than doubled at later time points indicating that the protein continued to diffuse away from the defect site.

To determine the effect of the hydrogel alone on bone regeneration, the extent of bone regeneration in the defects of mice treated with empty hydrogel was compared to bone regeneration in the defects of mice that received no treatment. The extent of bone regeneration was imaged by micro-computed tomography (μCT) on post-operative days 2, 5, and 14, and was quantified using advanced image processing algorithms [35]. We previously developed and validated these algorithms in order to segment bones of varying and heterogeneous mineral content, which are seen in the healing of this pediatric specific model of re-synostosis. There was a minor reduction of bone within the defect in mice treated with the hydrogel alone (Supplemental Figure S4). By 14 days post-op, there were no differences in either the average defect width or the volume of bone in the defect compared to empty defects. This indicates that our hydrogel has a space occupying effect early, but in vivo the empty gel has no long-term effect on bone regrowth. These results demonstrate that the gel is non-toxic to the cells responsible for bone regeneration and the hydrogel alone does not have a long-term effect on bone regeneration.

3.5 Effectiveness of hydrogel to deliver rmGremlin1 to delay re-synostosis

To address the clinical need in children who undergo surgical intervention for craniosynostosis, we used our click hydrogel to deliver the BMP inhibitor rmGremlin1 to delay the post-operative bone growth that occurs without any intervention in our weanling mouse model. Cranial defects were created over the posterior frontal suture in 21-day-old male mice and randomized to both the post-operative time point and treatment groups: empty defect, hydrogel + carrier (4 mM HCl), hydrogel + 300 ng rmGremlin1, hydrogel + 500 ng rmGremlin1, and un-polymerized PEG-N3 + 500 ng rmGremlin1. Mice were euthanized and imaged with μCT and histology on post-op days 5 and 14. Empty defects contained a thick trabeculated structure by 14 days post-op, which was visible on both the μCT and histological images. This defect was nearly completely bridged as seen with the 3D rendering, similar to what has been observed previously in this animal model (Figs. 4A–C) [31]. The defects containing the hydrogel exhibited the same thick trabeculated structure, but complete bridging was not evident along the midline (Figs. 4D–F). The 3D rendering showed that this small gap occurred in only a very small region and the majority of the defect was healed (Figure 4D). Histology of the site showed disorganized fibrous connective tissue between the bones of the defect (Figure 4F). Inclusion of rmGremlin1 in the hydrogel resulted in a dose dependent decrease in the amount of bone present in the defect (Figs. 4G–L). None of the animals in these groups displayed bridging of the defect and histology showed more fibrous connective tissue was present (Figs. 4I, L). Additionally, the 2D μCT images showed a lack of the thick trabecular structure noted above (Figure 4H, K). Defects containing the un-polymerized PEG-N3 also had nearly completed bridging of the defect and contained the thick trabecular structure observed in the empty defects on post-op day 14 (Figs. 4M–O), indicating that the highest dose of rmGremlin1 did not have an effect on defect healing in the absence of a cross-linked gel.

These observations were supported by quantitative analysis of the μCT images using our advanced segmentation algorithms described above. On post-op day 5, there was a decrease in the width of untreated defects and a slight decrease in the distance between bones for the hydrogel + carrier group. However, for both of the groups containing rmGremlin1, there was

no decrease from the initial 1.5 mm wide defect (Figure 5A). At 14 days post-op, the distance between bones in the hydrogel + carrier and hydrogel + 300 ng rhGremlin1 treatment groups decreased, but there was no change in defect width in sites treated with the hydrogel + 500 ng rmGremlin1, indicating that the effects of rmGremlin1 were dose dependent (Figure 5A). As seen previously, the empty defects were bridged early as no changes in distance between bones were observed between 5 and 14 days post-op [31]. Histomorphometric analysis of coronal sections cut through the center of the defect showed significantly wider defects at 14 days postop in the hydrogel + 500 ng rhGremlin1, but other differences were not present as the variability associated with the non-serial histomorphometry was greater as this only examined one section of the middle of the defect (Supplemental Figure S5). Cross-linking of the gel was necessary to retain rmGremlin1 at the site. PEG-N3 + 500ng rmGremlin1 had no impact on bone formation, as there were no differences at either time point between this group and the empty defect (Figure 5A). There were no differences among any of the groups on post-operative day 5 in the defect thickness, defect mineral content, and defect bone volume, as this time point is before the defect undergoes the mineralization that is part of normal defect healing (Figs. 5B–D). However, defect mineral content and bone volume were decreased in a dose-dependent manner on day 14 when rmGremlin1 was delivered in the crosslinked hydrogel. Both parameters increased on day 14 in the empty defects, in defects treated with hydrogel + carrier, and in defects treated with PEG-N3 + 500 ng rmGremlin1 (Figs. 5C–D). Additionally, there were no changes in any of the parameters between days 5 and 14 in sites treated with hydrogel + 500 ng rmGremlin1, indicating that no significant bone growth had occurred.

3.6 Long term performance of hydrogel to delay re-synostosis

The ultimate goal for any treatment of re-synostosis is to slow down, but not completely prevent the rapid post-operative bone growth that is commonly seen in children with craniosynostosis. To investigate the long-term effect of our hydrogel the same posterior frontal defect was created in 21-day-old male mice. The mice were randomized to receive an empty defect, hydrogel + carrier, hydrogel + 500 ng rmGremlin1. The mice were randomized for euthanasia at either 14 or 28 days and the extent of bone regeneration was assessed by μCT and histology. Similarly to what was seen above, the algorithm results showed that the average defect width was lower in the Empty and Hydrogel + Carrier groups and the defect width for the Hydrogel + 500 ng group did not change from the initial 1.5 mm (Figure 6A). By 28 days, the defect width decreased in the Hydrogel + 500 ng group and there were no differences among the groups by this later time point (Figure 6A). The average defect thickness was less in the Hydrogel + 500 ng group than the Empty defects at 14 days post-op, but there were no differences seen by 28 days post-op (Figure 6B). Both the defect mineral content and bone volume were lower in the Hydrogel + 500 ng group, as compared to both other groups, 14 days post-op (Figure 6C–D). By 28 days post-op, both parameters increased in the Hydrogel - 500 ng groups and there were no differences among any of the groups (Figure 6C–D). Similar differences among the groups were seen with the histomorphometric analysis for both the average defect width and average defect thickness.

4. Discussion

Our results clearly demonstrate that our click-hydrogel permits rapid in situ polymerization for controlled delivery of biologically active therapeutic proteins. Polymerization of PEG-N3 and the PEG-DBCO to form hydrogels resulted in very rapid crosslinking that occurred spontaneously via a bio-orthogonal click-based gelation mechanism that is unreactive to co-administered proteins and the surrounding tissues. The polymerization for all applications resulted in a fully cross-linked hydrogel in less than 90 seconds, which is almost two orders of magnitude faster than previously described click-based hydrogels [20]. Another major advantage of our click hydrogel is the ability to tailor the properties of the gel easily without modifying the chemistry of the components. This tremendous flexibility allows us to tailor the mechanical properties and release rate of the hydrogel making it suitable for numerous application. For our application, we were able to select a composition that was able to provide a controlled release of Gremlin1, for up to 14 days, which in turn was able to delay, but not prevent, the rate of postoperative bone growth.

The rapid spontaneous polymerization that is possible with our chemistry has the potential to deliver incorporated factors to any site that can be reachable with a needle. UV photopolymerization is perhaps the most widely used method to rapid form gels in situ. While this produces rapidly crosslinking gels, the toxicity associated with the UV radiation would be prohibitively toxic for the treatment for craniosynostosis, as any therapeutic polymer would have to be delivered directly onto the child's dura. This is of upmost concern on the developing brain because UV radiation is commonly used as a method to induce neuron apoptosis. Aside from the potential toxicity associated with UV radiation, the polymerization of these materials is further limited because the components must be exposed to the UV source in order to undergo polymerization. As a result, these materials cannot be delivered to deep tissues without performing an invasive surgical procedure. Another advantage of our bio-orthogonal click hydrogel is that the gel reactions that occur during polymerization should not interfere with any co-administered therapeutics or with the surrounding tissues. This was seen with the incorporated proteins retained their biological activity following in situ polymerization both in vitro and in vivo.

This is the first use of rmGremlin1 to delay the rapid bone growth that is seen in pediatric patients following cranial vault surgery. The hydrogel with rmGremlin1 was able to achieve a dose dependent inhibition in the rate of bone growth. The results from the long-term study demonstrated that the bone was able to regenerate partially by 28 days post-op. This demonstrates that our therapy was able to delay, but not completely prevent the rapid re-synostosis that is seen with the weanling murine model. Previous work in an adult murine cranial defect demonstrated that cells transfected to overexpress the BMP antagonist Noggin demonstrated some inhibition in the regeneration of bone in the defect [16]. The major drawback to this model is that adult animals do not experience rapid bone regeneration seen in identical defects created in weanling animals, thus limiting the applicability of the adult system to the clinical challenge of re-synostosis in infants [31]. Furthermore, this approach used cells transfected with retroviruses, which have significant barriers to becoming a viable therapy and have the potential for mutagenicity.

One of the challenges necessary to translate the hydrogel into use for humans is to extend the delivery period of the hydrogels. In mice, the re-synostosis occurs in two weeks, but in some children with craniosynostosis, it would be necessary to extend this duration to several months. Moving from a relatively thin (~200 μm) hydrogel in mice to a much thicker gel in humans would extend the release kinetics as the distance of diffusion would be much greater. Additionally, the plug and play architecture of the PEG-N3 RAFT polymerization would allow therapeutic molecules to be tethered covalently or ionically to the hydrogel, further extending the active duration of the therapy. Alternatively, it would be possible to do a series of repeated injections of the hydrogel to extend the duration while simultaneously lowering the dose of the therapeutic molecule delivered to the child at any one time. In addition to delivering BMP inhibitors, rapid in situ polymerization that occurs with this hydrogel would also allow the hydrogel to be used for other regenerative applications that may necessitate cell adhesion peptides, cleavable linkages, or covalent attachment of therapeutic small molecules.

Not only does our hydrogel therapy have tremendous potential to delay the post-operative re-synostosis frequently seen in cases of craniosynostosis and in turn reduce the risk of life threatening complications associated with additional surgical intervention for the treatment of re-synostosis. Early treatment of re-synostosis used physical and chemical barriers to prevent the post-operative bone growth but these were abandoned because they were ineffective and were associated with numerous complications [40–42]. The ultimate goal with any re-synostosis therapy is to slow the post-operative bone growth for a period, but then allow the bone to re-grow as the child aged.

5. Conclusions

If successful, the hydrogel therapy could also allow for the endoscopic removal of the fused suture and in effect re-create the function of a normal suture. Outside of craniofacial reconstruction, delaying the rate of bone growth has direct applications in treating fractures of the growth plate and heterotopic ossification. In addition to delivering BMP inhibitors, rapid in situ polymerization that occurs with this hydrogel would also allow the hydrogel to be used for other regenerative applications that may necessitate cell adhesion peptides, cleavable linkages, or covalent attachment of therapeutic small molecules. For this reason, we anticipate numerous applications of our click-based hydrogel in areas of drug delivery and tissue engineering.

Supplementary Material

Refer to Web version on PubMed Central for supplementary material.

Acknowledgments

This research was supported by grants from Children’s Healthcare of Atlanta and the Food and Drug Administration. This work was supported by the grants from the National Heart, Lung and Blood Institute of the NIH as a Program of Excellence in Nanotechnology award (HHSN268201000043C). In addition, this work was supported by R01HL096796-04 and R01AI088023-03.

References

1. Boulet SL, Rasmussen SA, Honein MA. A population-based study of craniosynostosis in metropolitan Atlanta, 1989–2003. Am J Med Genet A. 2008; 146A:984–991. [PubMed: 18344207]
2. Hunter AG, Rudd NL. Craniosynostosis. I. Sagittal synostosis: its genetics and associated clinical findings in 214 patients who lacked involvement of the coronal suture(s). Teratology. 1976; 14:185–193. [PubMed: 982314]
3. Hunter AG, Rudd NL. Craniosynostosis. II Coronal synostosis: its familial characteristics and associated clinical findings in 109 patients lacking bilateral polysyndactyly or syndactyly. Teratology. 1977; 15:301–309. [PubMed: 882919]
4. Lajeunie E, Le Merrer M, Bonaiti-Pellie C, Marchac D, Renier D. Genetic study of nonsyndromic coronal craniosynostosis. Am J Med Genet. 1995; 55:500–504. [PubMed: 7762595]
5. Kirman CN, Tran B, Sanger C, Railean S, Glazier SS, David LR. Difficulties of delayed treatment of craniosynostosis in a patient with Crouzon, increased intracranial pressure, and papilledema. J Craniofac Surg. 2011; 22:1409–1412. [PubMed: 21772166]
6. Panchal J, Uttchin V. Management of craniosynostosis. Plast Reconstr Surg. 2003; 111:2032–48. quiz 2049. [PubMed: 12711969]
7. Gosain AK, McCarthy JG, Wisoff JH. Morbidity associated with increased intracranial pressure in Apert and Pfeiffer syndromes: the need for long-term evaluation. Plast Reconstr Surg. 1996; 97:292–301. [PubMed: 8559811]
8. Gault DT, Renier D, Marchac D, Jones BM. Intracranial pressure and intracranial volume in children with craniosynostosis. Plast Reconstr Surg. 1992; 90:377–381. [PubMed: 1513883]
9. Baird LC, Gonda D, Cohen SR, Evers LH, LeFloch N, Levy ML, et al. Craniofacial reconstruction as a treatment for elevated intracranial pressure. Childs Nerv Syst. 2012; 28:411–418. [PubMed: 22068642]
10. Foster KA, Frim DM, McKinnon M. Recurrence of synostosis following surgical repair of craniosynostosis. Plast Reconstr Surg. 2008; 121:70e–76e.
11. Williams JK, Cohen SR, Burstein FD, Hudgins R, Boydston W, Simms C. A longitudinal, statistical study of reoperation rates in craniosynostosis. Plast Reconstr Surg. 1997; 100:305–10. [PubMed: 9252595]
12. Esparza J, Hinojosa J. Complications in the surgical treatment of craniosynostosis and craniofacial syndromes: apropos of 306 transcranial procedures. Childs Nerv Syst. 2008; 24:1421–30. [PubMed: 18769932]
13. Esparza J, Hinojosa J, Garcia-Recuero I, Romance A, Pascual B, Martinez de Aragon A. Surgical treatment of isolated and syndromic craniosynostosis. Results and complications in 283 consecutive cases. Neurocirugia (Astur). 2008; 19:509–29. [PubMed: 19112545]
14. Mehta VA, Bettegowda C, Jallo GI, Ahn ES. The evolution of surgical management for craniosynostosis. Neurosurg Focus. 2010; 29:E5. [PubMed: 21121719]
15. Cooper GM, Curry C, Barbano TE, Burrows AM, Vecchione L, Caccamese JF, et al. Noggin inhibits postoperative resynostosis in craniosynostotic rabbits. J Bone Miner Res. 2007; 22:1046–54. [PubMed: 17437358]
16. Cooper GM, Usas A, Olshanski A, Mooney MP, Losee JE, Huard J. Ex vivo Noggin gene therapy inhibits bone formation in a mouse model of postoperative resynostosis. Plast Reconstr Surg. 2009; 123:94S–103S. [PubMed: 19182668]
17. Mooney MP, Losken HW, Moursi AM, Bradley J, Azari K, Acarturk TO, et al. Anti-TGF-beta2 antibody therapy inhibits postoperative resynostosis in craniosynostotic rabbits. Plast Reconstr Surg. 2007; 119:1200–12. discussion 1213–5. [PubMed: 17496591]
18. Frazier BC, Mooney MP, Losken HW, Barbano T, Moursi A, Siegel MI, et al. Comparison of craniofacial phenotype in craniosynostotic rabbits treated with anti-Tgf-beta2 at suturectomy site. Cleft Palate Craniofac J. 2008; 45:571–582. [PubMed: 18956936]
19. Wang F, Li Z, Khan M, Tamama K, Kuppusamy P, Wagner WR, et al. Injectable, rapid gelling and highly flexible hydrogel composites as growth factor and cell carriers. Acta Biomater. 2010; 6:1978–1991. [PubMed: 20004745]

20. DeForest CA, Polizzotti BD, Anseth KS. Sequential click reactions for synthesizing and patterning three-dimensional cell microenvironments. Nat Mater. 2009; 8:659–664. [PubMed: 19543279]
21. Fournier E, Passirani C, Montero-Menei CN, Benoit JP. Biocompatibility of implantable synthetic polymeric drug carriers: focus on brain biocompatibility. Biomaterials. 2003; 24:3311–3331. [PubMed: 12763459]
22. Akdemir ZS, Kayaman-Apohan N, Kahraman MV, Kuruca SE, Gungor A, Karadenizli S. Preparation of biocompatible, UV-cured fumarated poly(ether-ester)-based tissue-engineering hydrogels. J Biomater Sci Polym Ed. 2011; 22:857–872. [PubMed: 20566062]
23. McCollum AT, Nasr P, Estus S. Calpain activates caspase-3 during UV-induced neuronal death but only calpain is necessary for death. J Neurochem. 2002; 82:1208–1220. [PubMed: 12358768]
24. Mendelev N, Witherspoon S, Li PA. Overexpression of human selenoprotein H in neuronal cells ameliorates ultraviolet irradiation-induced damage by modulating cell signaling pathways. Exp Neurol. 2009; 220:328–334. [PubMed: 19766117]
25. Cheng IH, Lin YC, Hwang E, Huang HT, Chang WH, Liu YL, et al. Collagen VI protects against neuronal apoptosis elicited by ultraviolet irradiation via an Akt/phosphatidylinositol 3-kinase signaling pathway. Neuroscience. 2011; 183:178–188. [PubMed: 21459131]
26. Bock VD, Perciaccante R, Jansen TP, Hiemstra H, van Maarseveen JH. Click chemistry as a route to cyclic tetrapeptide analogues: synthesis of cyclo-[Pro-Val-psi(triazole)-Pro-Tyr. Org Lett. 2006; 8:919–922. [PubMed: 16494474]
27. Fan Y, Deng C, Cheng R, Meng F, Zhong Z. In situ forming hydrogels via catalyst-free and bioorthogonal “tetrazole-alkene” photo-click chemistry. Biomacromolecules. 2013; 14:2814–2821. [PubMed: 23819863]
28. Jiang Y, Chen J, Deng C, Suuronen EJ, Zhong Z. Click hydrogels, microgels and nanogels: emerging platforms for drug delivery and tissue engineering. Biomaterials. 2014; 35:4969–4985. [PubMed: 24674460]
29. Walsh DW, Godson C, Brazil DP, Martin F. Extracellular BMP-antagonist regulation in development and disease: tied up in knots. Trends Cell Biol. 2010; 20:244–256. [PubMed: 20188563]
30. Ross JJ, Shimmi O, Vilmos P, Petryk A, Kim H, Gaudenz K, et al. Twisted gastrulation is a conserved extracellular BMP antagonist. Nature. 2001; 410:479–483. [PubMed: 11260716]
31. Hermann CD, Lawrence K, Olivares-Navarrete R, Williams JK, Guldberg RE, Boyan BD, et al. Rapid re-synostosis following suturectomy in pediatric mice is age and location dependent. Bone. 2013; 53:284–293. [PubMed: 23201269]
32. Warren SM, Brunet LJ, Harland RM, Economides AN, Longaker MT. The BMP antagonist noggin regulates cranial suture fusion. Nature. 2003; 422:625–629. [PubMed: 12687003]
33. Ning X, Guo J, Wolfert MA, Boons GJ. Visualizing metabolically labeled glycoconjugates of living cells by copper-free and fast huisgen cycloadditions. Angew Chem Int Ed Engl. 2008; 47:2253–2255. [PubMed: 18275058]
34. Hurst-Kennedy J, Boyan BD, Schwartz Z. Lysophosphatidic acid signaling promotes proliferation, differentiation, and cell survival in rat growth plate chondrocytes. Biochim Biophys Acta. 2009; 1793:836–46. [PubMed: 19233232]
35. Hermann CD, Richards MA, Olivares-Navarrete R, Williams JK, Guldberg RE, Skrinjar O, et al. Algorithm to assess cranial suture fusion with varying and discontinuous mineral density. Ann Biomed Eng. 2012; 40:1597–1609. [PubMed: 22350663]
36. Lee SY, Pereira BP, Yusof N, Selvaratnam L, Yu Z, Abbas AA, et al. Unconfined compression properties of a porous poly(vinyl alcohol)-chitosan-based hydrogel after hydration. Acta Biomater. 2009; 5:1919–25. [PubMed: 19289306]
37. Gazzerro E, Pereira RC, Jorgetti V, Olson S, Economides AN, Canalis E. Skeletal overexpression of gremlin impairs bone formation and causes osteopenia. Endocrinology. 2005; 146:655–665. [PubMed: 15539560]
38. Hsu DR, Economides AN, Wang X, Eimon PM, Harland RM. The Xenopus dorsalizing factor Gremlin identifies a novel family of secreted proteins that antagonize BMP activities. Mol Cell. 1998; 1:673–83. [PubMed: 9660951]

39. Bretaudiere, JPST. Alkaline phosphatases. In: HUB, editor. Methods of Enzymatic AnalysisWeinheim. Germany: Verlag Chemie; 1984. p. 75-92.

40. Anderson F, Johnson F. Craniosynostosis; a modification in surgical treatment. Surgery. 1956; 40:961–970. [PubMed: 13371461]

41. Ingraham FD, Alexander E, Matson DD. Clinical studies in craniosynostosis analysis of 50 cases and description of a method of surgical treatment. Surgery. 1948; 24:518–541. [PubMed: 18884128]

42. Simmons DR, Peyton WT. Premature closure of the cranial sutures. J Pediatr. 1947; 31:528–547. [PubMed: 20268813]

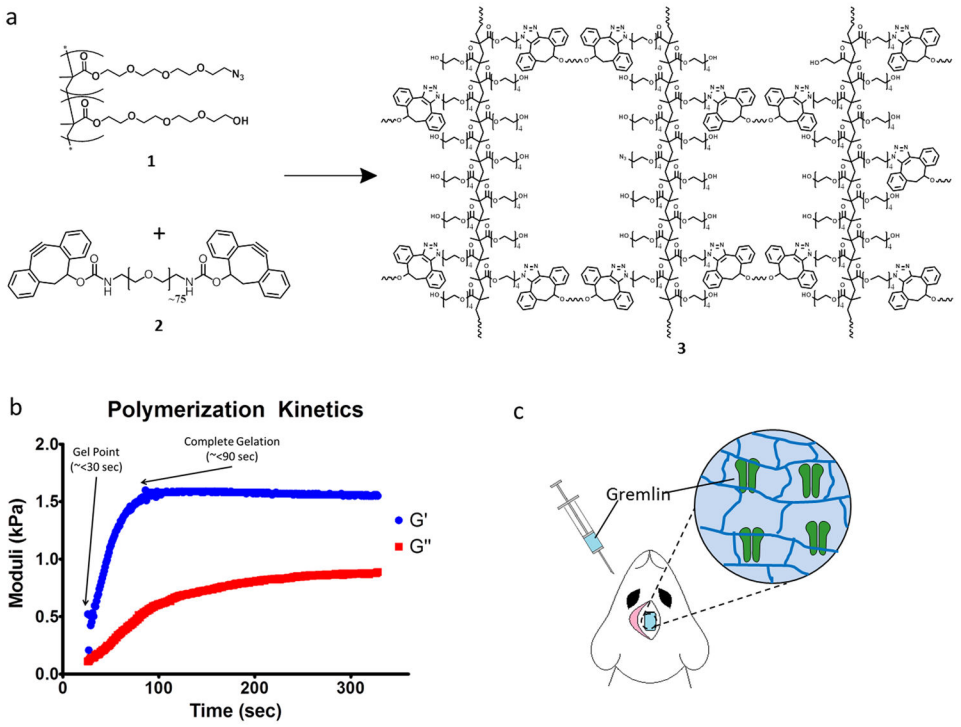

Figure 1.

Hydrogels formulated from azide functionalized PEG polymers and DBCO functionalized PEG crosslinker gel in less than two minutes. **A.** Azide-functionalized RAFT-copolymer (PEG N3) **1** rapidly crosslinks with PEG-DBCO crosslinker **2** via the [3 + 2] Huisgen cycloaddition to form a hydrogel. **1** and **2** react fast enough to allow for injection into tissue, hydrogel formation and biomolecule encapsulation. **B.** Spinning disk rheometry was used to determine the crosslinking dynamics of the hydrogel, and demonstrate that when mixed together, the two components begin to gel in less than 25 s with complete gelation occurring in less than 90 s. **C.** Cartoon illustrating the co-administration of rmGremlin1, **1**, and **2**, to a non-critical cranial defect and the subsequent entrapment of rmGremlin1 upon in situ crosslinking.

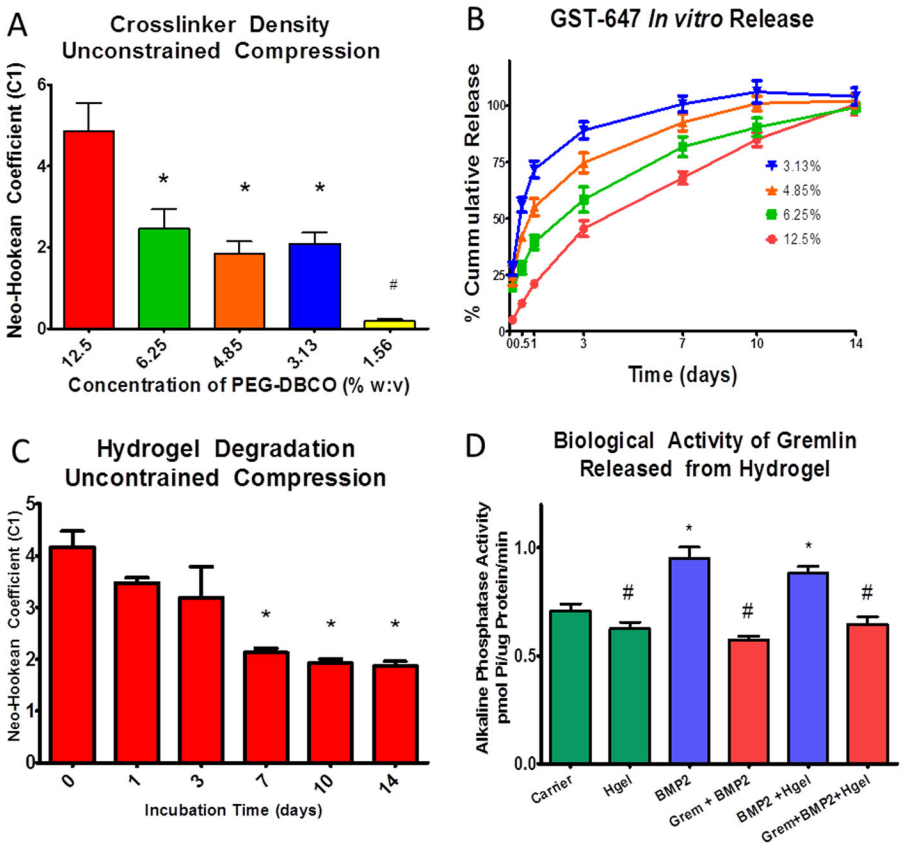

Figure 2.

Unconstrained compression testing of hydrogel using a Neo-Hookean hyperelastic model showed that increasing the concentration of the DBCO-PEG resulted in an increase in the Neo-Hookean coefficient (C1) (**A**) *=p<0.05 vs 12.5%. In vitro release of GST-647 from hydrogels with increasing concentrations of DBCO-PEG resulted in a more prolonged and linear release profile with the 12.5% gel having controlled release out to 14 days (**B**). Degradation of the 12.5% gel assessed by unconstrained compression had a decrease in the Neo-Hookean Coefficient after day 7 (**C**) *=p<0.05 vs day 0. The biological activity of rmGremlin1 was retained after release following polymerization in the hydrogel as assessed by blocking the BMP-2 mediated increase in alkaline phosphatase specific activity (**D**) *=p<0.05 vs carrier, #= p<0.05 vs BMP2.

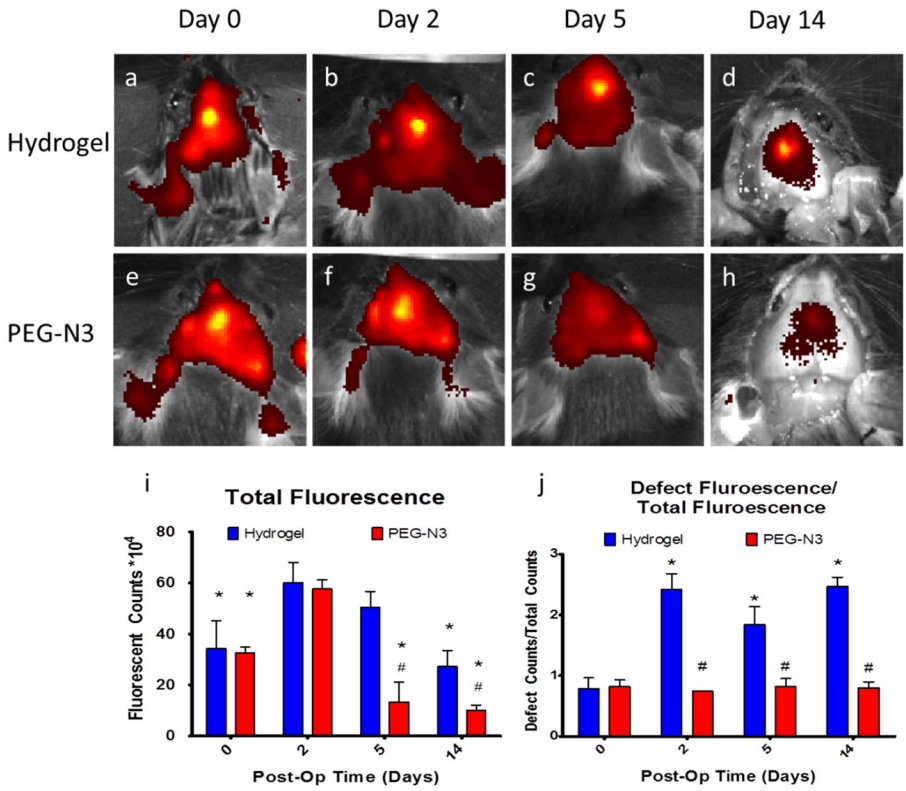

Figure 3.

In vivo fluorescence release of GST-647 kinetics following in situ polymerization of the hydrogel. Fluorescent images of mice with GST-647 in crosslinked hydrogel showed a controlled and localized signal over the defect up to 14 days after administration (**A–D**). In contrast, the signal of the group containing the un-polymerized PEG-N3 (**E–H**) showed relatively low levels of fluorescence after 5 and 14 days, demonstrating that, in the absence of crosslinking, the protein rapidly diffused out of the defect. Quantification of the total fluorescent signal over the entire head shows that 2 days after surgery there is more signal in the hydrogel gel group as compared to the PEG-N3 group and there is only a slight decrease in the total fluorescent signal (**I**) *=$p<0.05$ vs day 2, #=$p<0.01$ vs hydrogel. Comparing the ratio between the fluorescent signal in the defect to the total signal showed that the hydrogel groups had a higher fluorescence intensity 2 to 14 days after surgery, indicating that the hydrogel orchestrated a controlled release of incorporated protein (**J**) *=$p<0.05$ vs day 0, #=$p<0.05$ vs hydrogel.

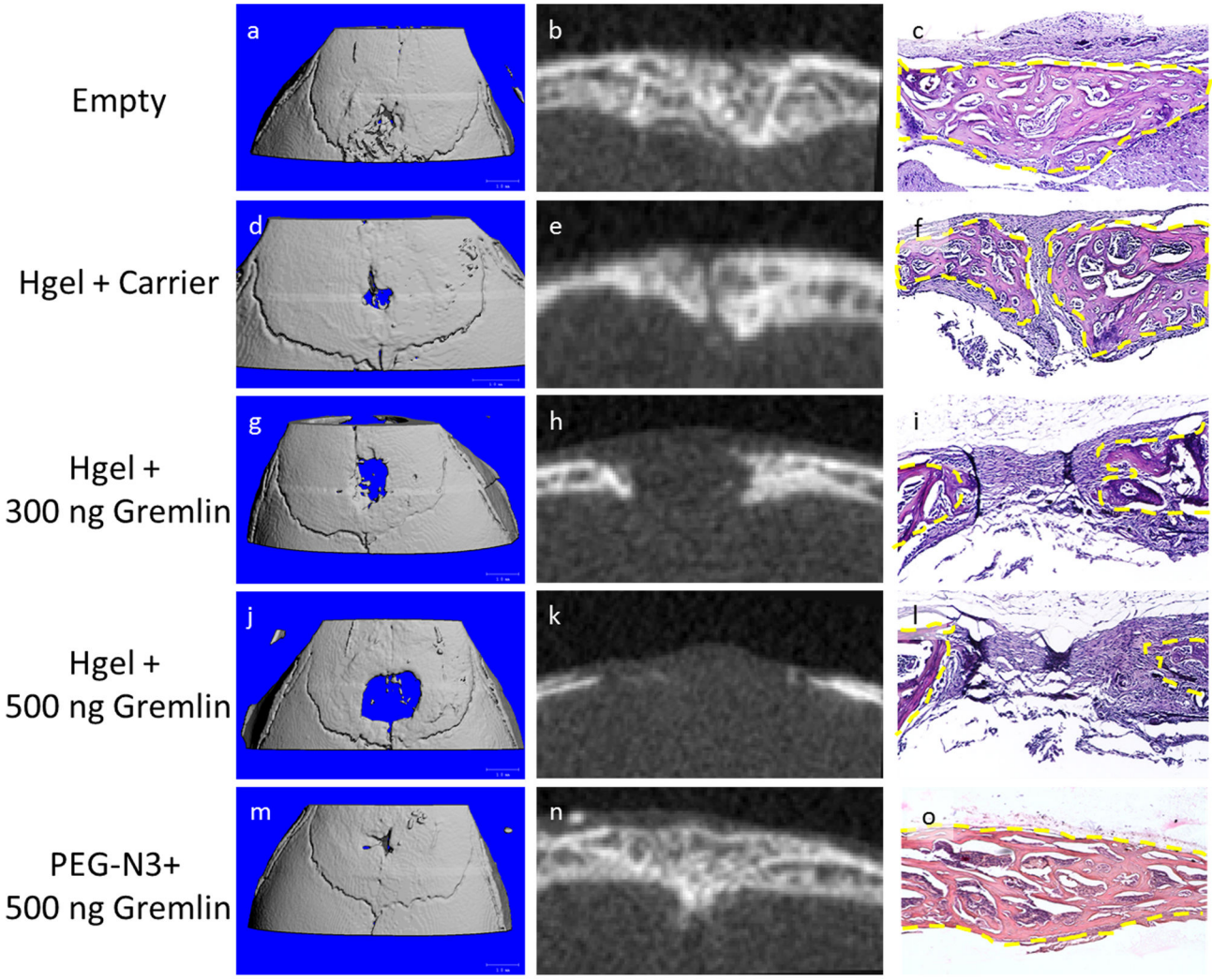

Figure 4.

Representative μCT and histology from 14 day post-op samples. Empty defects were nearly completely healed and bone bridging the defect (A–C). Defects with the hydrogel had very small regions that remained open, but there was thick trabecular bone present (D–F). Defects containing the hydrogel with rmGremlin1 showed a dose dependent decrease in the amount of bone present (G–L). The defects containing the low 300 ng dose showed no bone bridging of the defect (G–I), but the ends of the bone were thicker than the 500 ng group (J–L). The defects containing 500 ng rmGremlin1 in the un-polymerized PEG-N3 showed complete bridging and the same thick trabecular structure that was seen in the empty defect (M–O).

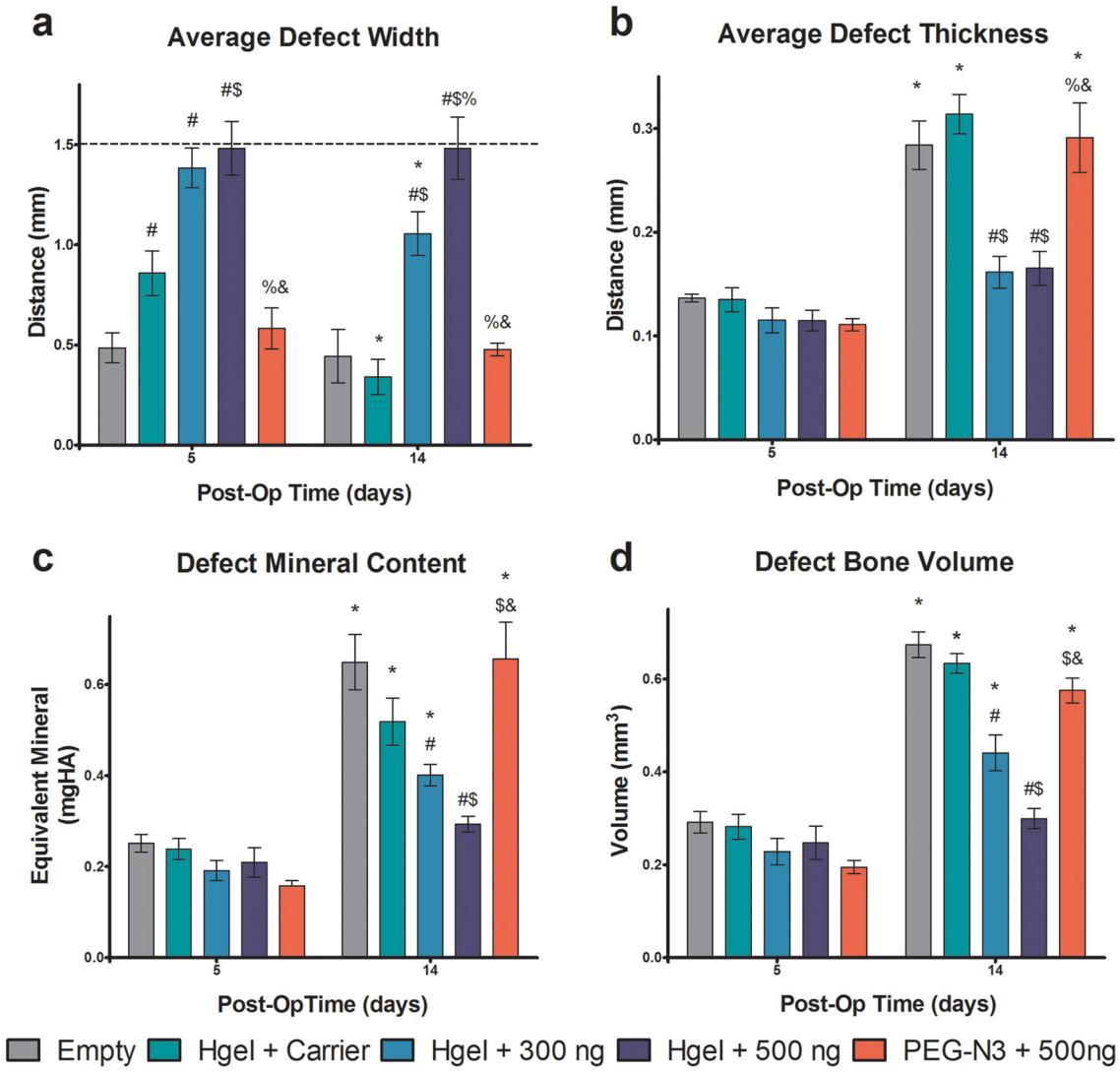

Figure 5.

Quantification of bone regeneration in defect by μCT imaging algorithm. Defects were left empty (Empty) on injected with hydrogel with 4 nM HCl carrier (Hgel + Carrier), hydrogel with 300 ng rmGremlin1 (Hgel + 300 ng), hydrogel with 500 ng rmGremlin1 (Hgel + 500 ng), or un-polymerized PEG-N3 with 500 ng rmGremlin1 (PEG-N3 + 500 ng). The average defect width had a dose dependent decrease on post-op day 14 and there was no change from the initial 1.5 mm defect (dashed line) for the Hgel + 500 ng group (**A**). The average defect thickness increased for all groups except the Hgel+300 ng and Hgel + 500 ng groups (**B**). Both the defect mineral content and bone volume showed a dose dependent decrease for the groups containing rmGremlin1 and there was no change in the Hgel + 500 ng groups (**C–D**). There were no differences between the Empty and PEG-N3 + 500 ng groups in any of the measures at either time point. $P<0.05$ vs. # = empty, $ = Hgel + Carrier, % = Hgel + 300 ng, & = Hgel + 500 ng, * = 5 days.

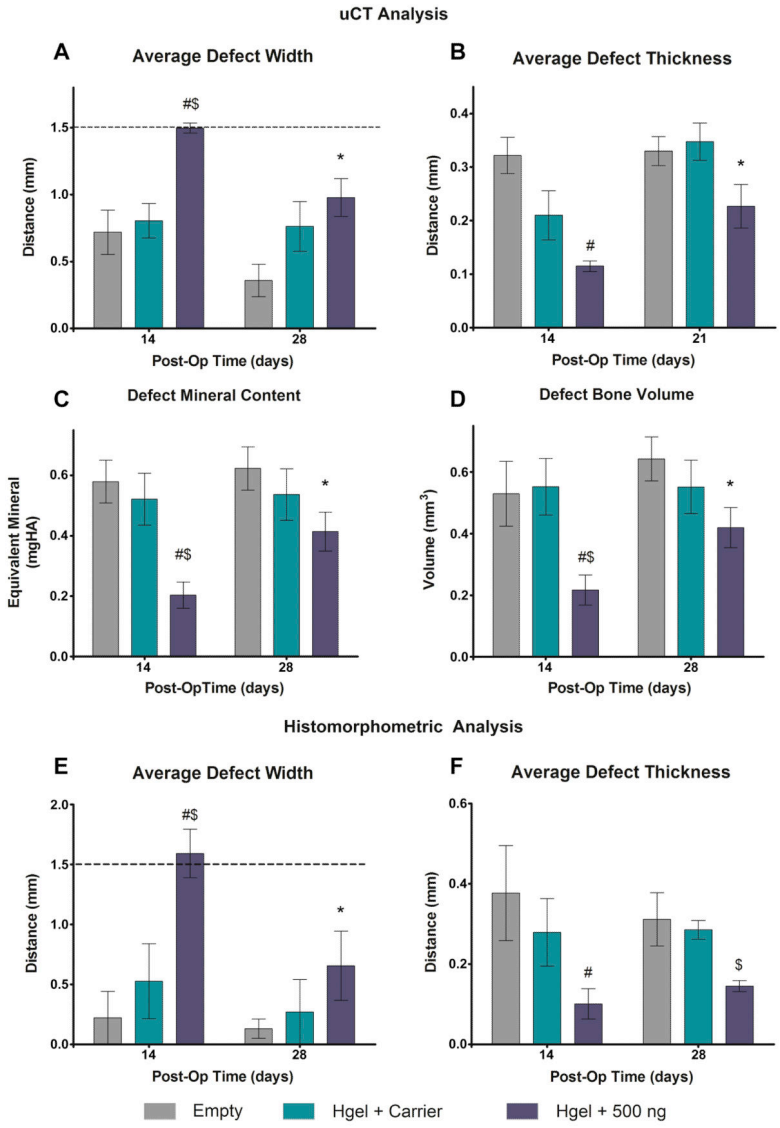

Figure 6.

Quantification of bone regeneration for extended time periods using imaging algorithm. Defects were left empty (Empty) on injected with hydrogel with 4 nM HCl carrier (Hgel + Carrier), or hydrogel with 500 ng rmGremlin1 (Hgel + 500 ng). The average defect width showed no differences between the Empty or Hydrogel + Carrier groups, but was significantly wider in the Hydrogel + 500 ng group by 14 days, but no differences by 28 days (A). The average defect thickness was lower in the Hydrogel + Gremlin, as compared to the empty defects, on 14 days postop, but there were no differences by 21 days (B). On 14 days post-op the Hydrogel + 500ng group had less mineral content and bone volume than either the Empty or Hydrogel + Carrier, but there were no differences among the groups at 28 days (C–D). Similar differences among the groups were also seen with histomorphometric analysis (E–F). $P<0.05$ vs. # = empty, $ = Hgel + Carrier, * = 14 days.